

基于 ResNeXt 网络的扰动轨道角动量谱识别

吴琼, 李海英*, 丁炜, 白璐, 吴振森

西安电子科技大学物理与光电工程学院, 陕西 西安 710071

摘要 涡旋波束携带的轨道角动量(OAM)模态在通信容量提高、同时同频多路信息调制等领域具有重要的应用前景,但涡旋波束经复杂介质环境后会造成波束场幅度和相位扰动,进而引起信道串扰、高误码率等问题。基于 ResNeXt 网络,提出了一种基于实测涡旋波束扰动场的图像,识别扰动场 OAM 谱分布的方法。以涡旋贝塞尔波束入射玻璃板的实验图像为例,利用所提方法进行 OAM 谱识别,对于不同入射方向情况下的场幅度图像,通过优化后的 ResNeXt 网络获得了透射场的 OAM 谱分布结果,对识别结果进行谱分布重构,并与数值计算结果进行对比,分析误差。结果表明,优化后的 ResNeXt 网络可以有效地识别出穿过玻璃介质之后的入射角为 $0^\circ \sim 45^\circ$ 的贝塞尔波束的透射场 OAM 谱分布,由于谱分布的弥散程度随着入射角度的增大而增大,与理论计算结果相比,主模相对误差亦随角度的增大而增大,但最大不超过 22.86%。

关键词 光通信; 涡旋贝塞尔波束; 轨道角动量; 螺旋谱; 神经网络; 透射场

中图分类号 TN929.1; TP181

文献标志码 A

doi: 10.3788/CJL202148.1706003

1 引言

涡旋波束是具有螺旋型相位波前和空心环状强度分布的特殊光场,它携带的轨道角动量(OAM)是具有相位因子 $\exp(il\varphi)$ (l 为拓扑荷数, φ 为波束方位角)的螺旋形波前光束特有的物理属性,同时涡旋波束具有正交性、涡旋性及多拓扑荷特性。这些特性决定了其在提高通信容量和雷达探测性能、自由空间激光通信及激光雷达遥感等领域具有重要的应用前景。

涡旋波束在复杂环境中传播时,场幅度和相位发生扰动,造成 OAM 谱分布异常。例如在大气湍流中传播时,波束会发生展宽^[1]、漂移^[2]、光强闪烁效应^[3]等,这些效应会对波束复振幅造成破坏、干扰 OAM 态的正交性,从而降低空间光通信系统的误码率性能。2016 年,柯熙政等^[4]研究了部分相干涡旋光束在大气湍流中传输时的光强分布,结果表明光强分布与传输距离、拓扑荷数及湍流强度有密切关系;2018 年,该团队^[5]分析了大气湍流下 OAM 复用态串扰问题,发现在湍流影响下 OAM 复用态光强有明显的闪烁现象且相位发生旋转弯曲,OAM

复用态之间的弥散程度随湍流强度的增大而增大。2020 年,闫玠霖等^[6]研究了大气湍流信道中聚焦涡旋光束 OAM 串扰特性,结果表明,OAM 间的串扰程度随着传输距离、湍流强度、拓扑荷数的增大和湍流内尺度、光束波长的减小而增大。此外,等离子体环境、复杂介质等也会造成涡旋波束传输的 OAM 谱扰动,例如,吕强等^[7]研究了左手介质中涡旋电磁波束的涡旋特性,结果表明左手介质中的逆古伊相移会导致涡旋波束的横向场和相应相位旋转方向反转;Pei 等^[8]发现贝塞尔高斯光束在梯度折射率介质中传输时,波束强度随着束腰半径的增大而增强,且波束在梯度折射率介质中的传输呈周期性;Li 等^[9]基于圆柱矢量波函数展开方法,研究了矢量贝塞尔波束在单轴各向异性平板、分层单轴各向异性平板^[10]上的反射和透射特性,基于角谱展开方法,研究了拉盖尔-高斯光束^[11]、矢量贝塞尔涡旋光束在各向同性介质板^[12]中的反射和透射特性等。结果表明,不论传输介质是各向同性还是单轴各向异性,涡旋波束反射场的幅度、相位分布和极化对波束入射角和介质介电特性等参数的敏感程度高于透射场,畸变更加明显,OAM 串扰程度更高。

收稿日期: 2021-01-15; 修回日期: 2021-02-10; 录用日期: 2021-03-09

通信作者: *lihy@xidian.edu.cn

大量研究表明,复杂介质环境造成的 OAM 谱扰动是 OAM 复用技术中需解决的关键问题之一。由数值计算方法不难获得涡旋波束 OAM 谱分布,但在实际测量系统中,如何根据实测场精准反演 OAM 谱的模式分布仍值得深入探讨。由于不同阶数的 OAM 波束有着不同的物理表现(如幅度图样),故可将 OAM 谱所包含的模式识别转换为图像分类问题。从人工神经网络-轨道角动量(ANN-OAM)模式分类器^[13]到卷积神经网络-轨道角动量(CNN-OAM)模式分类器,国内外学者做了很多尝试,ANN 由于无法学习相邻像素点的关联性,识别准确率较低而被 CNN 取代。目前使用较多的模式分类器包括误差反向传播(BP)神经网络模式分类器、支持向量机(SVM)模式分类器^[14]、CNN-OAM 模式分类器^[15-16]、全光衍射深度神经网络(D2NN)模式分类器^[17]等。相比于 ANN-OAM 模式分类器,CNN-OAM 模式分类器虽然识别准确率有了明显提高,但实验表明深度神经网络会出现退化问题,即网络深度增加时,网络准确度趋于饱和甚至开始下降。ResNet 加入了残差学习来解决退化问题,而 ResNeXt^[18]借鉴 inception 网络^[19]的架构对 ResNet 进行了改进,保持与 ResNet 相同精度的同时,提高了训练收敛速度,且 ResNeXt 网络结构更简单,可防止

对特定数据集的过拟合,便于自定义和修改。

本文基于 ResNeXt 网络,通过优化损失函数,对穿过玻璃介质的贝塞尔涡旋波束的透射场 OAM 谱分布进行了分类识别。目前大多关于 OAM 模式分类的文献主要针对主模的 OAM 模态进行检测,而所提方法在检测主模类别的基础上,将涡旋波束 OAM 谱分布问题转换为 CNN 中识别测试样本属于每类训练样本的概率问题,由此得到主模及主要旁瓣 OAM 模态所占百分比情况,为 OAM 模式识别提供了一种新的思路。

2 基于 ResNeXt 网络的 OAM 谱识别方法

2.1 基于 ResNeXt 网络的 OAM 谱识别流程

在所研究的问题中,训练样本为阶数 4~12、未穿过玻璃介质、没有发生畸变的贝塞尔波束光强图样,测试样本为实验得到的不同入射角情况下 8 阶贝塞尔波束穿过玻璃介质的光强图。ResNeXt 网络首先对测试样本所属类别进行检测,即主模识别,然后令网络学习对应预置的 OAM 谱分布拟合函数,得到测试样本属于每类训练样本的概率,以此达到重构波束透射场 OAM 谱分布的目的,具体识别流程如表 1 所示。

表 1 基于 ResNeXt 网络的贝塞尔波束透射场 OAM 谱识别流程

Table 1 OAM spectrum identification process of Bessel beam transmission field based on ResNeXt network

Layer	Type	Detail
1	Input	Input is typically 64×64 grayscale image
2	2D Convolution	Eight 3×3 filters with stride 1, padding "same"
3	Batch normalization	
4	Rectified linear units	
5	Max pooling	2×2 max pooling with stride 2
6	2D Convolution	Eight channels, 163×3 filters, stride 1, padding "same"
7	Batch normalization	
8	Rectified linear units	
9	Max pooling	2×2 max pooling with stride 2
10	2D Convolution	16 channels, 323×3 filters, stride 1, padding "same"
11	Batch normalization	
12	Rectified linear units	
13	Fully connected	8912 inputs and 9 outputs
14	Softmax	
15	Classification with OAM spectrum distribution prediction	9 classes with cross-entropy loss function, smooth L1 loss, $f(l)$

2.2 损失函数选择

损失函数是模型对数据拟合程度的反映,是神经网络的关键组成部分,不仅要反映出求解问题的真实标签,而且要有合理的梯度。梯度求解有利于对权重和参数进行更新。所提方法的损失函数由 3 部分组成:

$$L_{\text{total}} = L_1 + L_2 + L_3, \quad (1)$$

式中: L_1 为交叉熵函数; $L_2 + L_3$ 为预测 OAM 谱分布的损失函数。

L_1 计算的是测试样本主模分类损失,交叉熵函数是分类问题中常用的损失函数之一,表达式为

$$H(p, q) = - \sum_{i=1}^n p(x_i) \log [q(x_i)], \quad (2)$$

式中:概率分布 p 为期望输出;概率分布 q 为实际输出; n 为训练数据的总数; x 为训练样本。交叉熵表征实际输出和期望输出的距离,即交叉熵的值越小,两个概率分布就越接近。在分类问题中,交叉熵常常与 Softmax 是标配,Softmax 对输出的结果进行处理,使多个分类的预测值和为 1,再通过交叉熵

表 2 贝塞尔波束透射场 OAM 谱分布

Table 2 OAM spectrum distribution of Bessel beam transmission field

Incident angle	$l=4$	$l=5$	$l=6$	$l=7$	$l=8$	$l=9$	$l=10$	$l=11$	$l=12$
$\theta=0^\circ$			7.80×10^{-6}	4.04×10^{-4}	0.9989	3.92×10^{-4}	7.75×10^{-6}		
$\theta=10^\circ$			0.007	0.002	0.9822	0.0017	0.0066		
$\theta=20^\circ$			0.1073	0.0066	0.7703	0.006	0.1013		
$\theta=30^\circ$	0.0757	0.0073	0.3301	0.0089	0.1684	0.0085	0.3120	0.0065	0.0662
$\theta=40^\circ$	0.2198	0.0111	0.0574	0.0071	0.1020	0.0068	0.0577	0.01	0.2177

表 3 不同入射角情况下拟合函数参数

Table 3 Fitting function parameters under different incident angles

Incident angle	a_0	a_1	b_1	ω
$\theta=0^\circ$	0.3331	-0.3339	-0.576	2.094
$\theta=10^\circ$	0.3297	-0.3129	-0.5725	2.097
$\theta=20^\circ$	0.2819	0.042	-0.4866	2.17
$\theta=30^\circ$	0.1249	0.0003072	-0.1093	1.768
$\theta=40^\circ$	0.0722	-0.0509	-0.0211	2.403

L_3 与 L_1 相同,为交叉熵函数,网络学习参数完毕后经过 Softmax 层处理输出测试样本属于每类训练样本的概率。

来计算损失。

确定了测试样本主模类别后,下一步为预测 OAM 谱分布。 $L_2 + L_3$ 为预测 OAM 谱分布的损失函数,其中 $L_2 = f(l) + L_{\text{smooth } L1}$ ^[20], $L_{\text{smooth } L1}$ 为典型常用损失函数, $f(l)$ 为自定义损失函数。 $f(l)$ 是根据涡旋波束谱分析理论^[21-22] 计算得到的波束透射场 OAM 谱分布图像拟合而来的函数,由于输入强度图像的 CNN 特征与旁瓣的关联性弱,设置此函数的目的在于减小谱分布预测结果与数值计算结果间的误差,提高识别精度,表达式为

$$f(l) = a_0 + a_1 \times \cos(\omega l) + b_1 \times \sin(\omega l), \quad (3)$$

式中: a_0, a_1, b_1, ω 为损失函数的固定参数。不同入射角情况下谱分布图像不同,对应的固定参数不同。当入射贝塞尔波束的阶数为 8,入射角 θ 分别为 $0^\circ, 10^\circ, 20^\circ, 30^\circ, 40^\circ$ 时,由螺旋谱分析理论计算得到的主要模态占比如表 2 所示,其中入射角为 $0^\circ, 10^\circ, 20^\circ$ 情况下占比小于 10^{-6} 的模态忽略不计。将表 2 中拓扑荷数 l 和对应角度下的模态占比 $f(l)$ 代入(3)式,得到的自定义损失函数固定参数如表 3 所示。

3 实例分析

3.1 贝塞尔涡旋波束入射玻璃板的透射场实验

产生涡旋波束的方法除了常见的空间光调制器^[23]、计算全息法^[24-25]、螺旋相位板法^[26],近年来学者们还利用变形镜^[27]、损耗点镜^[28]、径向相移螺旋型波带片(RSSZP)^[29]等制备涡旋波束。本实验组基于螺旋相位板法产生了 1 阶和 8 阶的高阶贝塞尔涡旋波束,并使该波束通过厚度为 4 mm 的玻璃介质,得到透射场光强分布图。实验装置如图 1 所示,其中 A 为氦氖激光器,可产生 632.8 nm 波长的高斯波束;B 为双元件偏振架,装有偏振片 P1 和 P2,可以将从激光器出来的高斯波束转变为线偏振态,还可以调节 COMS 相机所接收到的波束功率;C 为准直扩束器,由凸透镜 T1 和 T2 组成;D 为圆形

光阑,通过调节通光孔径,可以近似认为高斯波束光轴中心部分是平面波;E 是型号为 AX255-A 的轴锥镜(锥角为 5°),可产生半锥角为 2.314° 的零阶贝塞

尔波束;F 为螺旋相位板;G 是厚度为 4 mm,折射率为 1.38 的均匀各向同性玻璃板;H 为 COMS 相机,用来观察贝塞尔波束的光强分布。

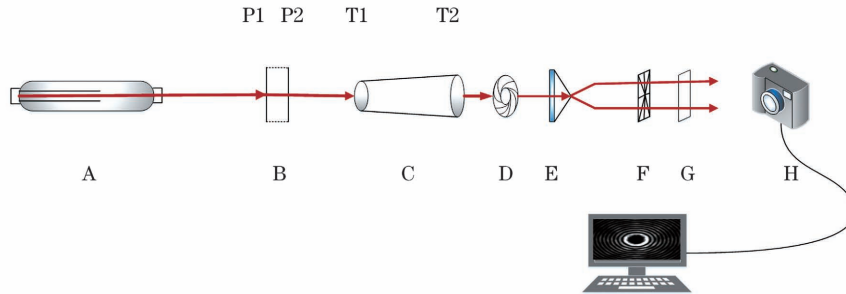


图 1 基于螺旋相位板方法产生高阶贝塞尔波束的实验装置示意图

Fig. 1 Schematic diagram of experimental device for generating high-order Bessel beam based on spiral phase plate method

实验观测到的 0 阶、1 阶、8 阶贝塞尔波束光强图如图 2 所示,可以看到贝塞尔波束中心圆环直径随着波束阶数的增大而增大。

8 阶贝塞尔波束以不同入射角度穿过玻璃介质后的透射场光强分布如图 3 所示,由于贝塞尔波束可以看成沿各个方向传播的平面子波叠加,当其斜入射各向同性玻璃板时,这些平面子波的波矢拥有不同的

入射角。折射角与透射角也都不一致,因此强度图样不能保持圆对称结构,中心圆环发生了明显的形变,且形变程度随着入射角的增大而增大,当入射角度增大到一定程度时,形变产生的椭圆光环的两个长弧部分互相连接在一起,形成了一个“梳子”型结构。入射角为 20° 、 30° 时,COMS 相机距玻璃板约 5.5 cm。其他 3 种情况下,COMS 相机距玻璃板约 5 cm。

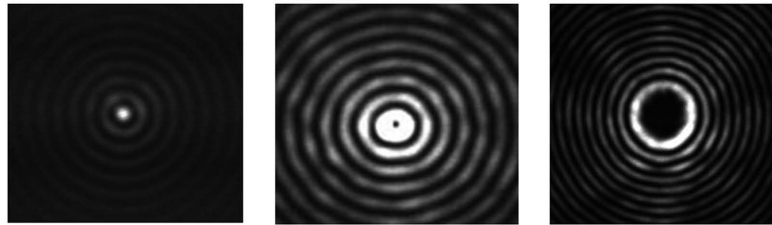


图 2 0 阶、1 阶、8 阶贝塞尔波束光强图

Fig. 2 Intensity diagram of 0-order, 1st-order, 8th-order Bessel beam

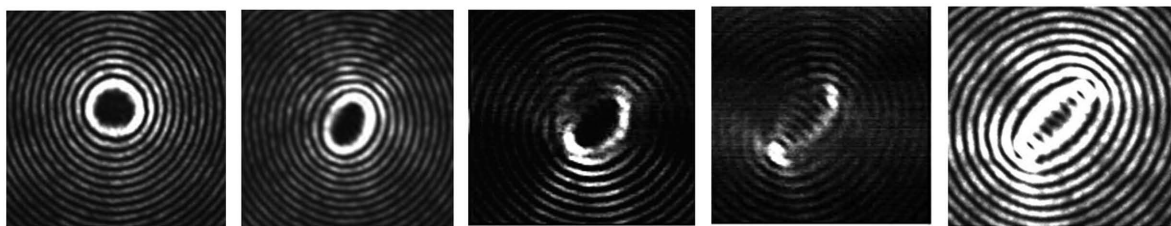


图 3 8 阶贝塞尔波束分别以 0° 、 10° 、 20° 、 30° 、 40° 的入射角穿过玻璃介质后的透射场光强分布图

Fig. 3 Intensity distribution diagram of transmission field of the eighth-order Bessel beam passing through the glass medium at the incident angles of 0° , 10° , 20° , 30° , 40° , respectively

3.2 图像识别结果与数值计算结果对比

基于表 1 的识别流程,以图 3 中不同入射角情况下的 8 阶贝塞尔波束透射场光强图为测试样本,训练图片的尺寸为 $140 \text{ pixel} \times 140 \text{ pixel}$,训练样本共 9 类,每类有 20 张图片。为防止过拟合,模型训练步数为 250,训练时间为 63 min。对基于 ResNeXt 网络的贝塞尔波束透射场 OAM 谱识别

结果与表 2 中的数值结果进行了对比,结果如图 4 所示。

由图 4 可以看出:贝塞尔波束透射场 OAM 谱分布弥散程度随入射角的增大而增大,当入射角增大到一定程度时,主模失去主导地位,旁瓣占比超过了主模,谱分布规律性减弱;ResNeXt 网络的识别误差也随入射角的增大呈增长趋势。

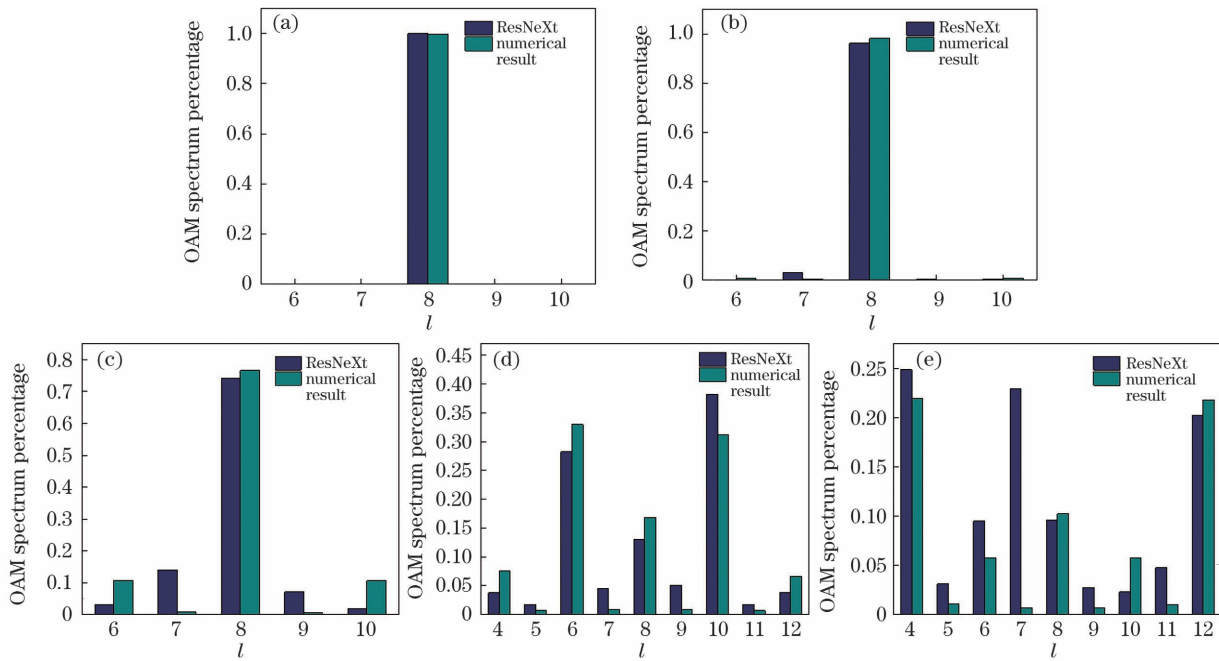


图 4 OAM 谱识别值与数值结果对比。(a)~(e) $\theta=0^\circ, 10^\circ, 20^\circ, 30^\circ, 40^\circ$

Fig. 4 Comparison of OAM spectrum recognition value and numerical result. (a)~(e) $\theta=0^\circ, 10^\circ, 20^\circ, 30^\circ, 40^\circ$

3.3 识别方法精度分析讨论

ResNeXt 网络综合了 VGG 网络和 inception 网络的优势,在增加准确率的同时减少了参数的数

量,降低了模型的复杂度,网络的可扩展性较好。对 8 阶贝塞尔波束透射场主模识别值和表 2 的数值计算结果进行了对比,如表 4 所示,并计算了相对误差。

表 4 8 阶贝塞尔波束主模实测值和数值计算结果对比

Table 4 Comparison of measured values and numerical calculation results of the eighth-order Bessel beam main mode

Incident angle	$\theta=0^\circ$	$\theta=10^\circ$	$\theta=20^\circ$	$\theta=30^\circ$	$\theta=40^\circ$
ResNeXt	0.9999	0.9619	0.7420	0.1299	0.0961
Numerical result	0.9989	0.9818	0.7660	0.1684	0.1020
Relative error / %	0.10	-2.03	-3.13	-22.86	-5.78

由表 4 可以看出,基于 ResNeXt 网络的主模识别精度随着入射角的增大有所下降,但与数值结果比较的相对误差最大不超过 22.86%,旁瓣绝对误差不超过 22.23%。误差来源主要有 3 方面:首先由于贝塞尔波束具有多拓扑荷特性,OAM 谱分布以主模位置为中心向两边无限延伸,但训练集类别是有限的,只能对占比较大的模态进行讨论;其次贝塞尔波束透射场 OAM 谱分布规律性随着入射角的增大而减弱,弥散越来越明显,导致识别精度降低;由于 OAM 谱识别问题和常规的分类问题不同,测试样本的 CNN 特征与主模较为相关而与旁瓣关联性较弱,自定义损失函数虽起到了减小误差的作用,但是并不能决定网络的识别结果,因此旁瓣识别误差大于主模。

4 结 论

基于 ResNeXt 网络,通过引入自定义损失函

数,对入射角在 $0^\circ \sim 45^\circ$ 内的穿过玻璃介质的贝塞尔波束的透射场 OAM 谱分布进行了识别,并与数值结果进行了对比和误差分析。结果表明,主模相对误差随着波束入射角的增大而增大,但不超过 22.86%,旁瓣识别误差大于主模。此外,所提方法同样适用于传输介质厚度变化和传输介质非均匀的情况。因为玻璃板厚度变化对贝塞尔波束透射场 OAM 谱分布的影响规律同入射角变化对其的影响规律相似,当入射角不变,OAM 谱的弥散程度随着玻璃板厚度的增加而增大,当增大到一定程度时,旁瓣占比超过主模,因此引入的自定义损失函数依然适用。且当贝塞尔波束在非均匀介质中传输时,可以根据波束透射场 OAM 谱分布图像规律调整自定义损失函数的形式,使网络适用于非均匀传输介质中的 OAM 谱识别。例如,贝塞尔波束在尘埃等离子体中传输时,透射场 OAM 谱分布特征符合高斯分布,可将自定义函数设置为高斯函数,以达到识别贝塞尔

波束穿过尘埃等离子体后的透射场 OAM 谱分布的目的。所提方法不再局限于波束主模的分类识别,而是对波束 OAM 谱分布主模百分比进行了具体识别,为 OAM 模式识别问题提供了一种新的思路,而如何进一步提高旁瓣的识别准确率是下一个挑战。

参 考 文 献

- [1] Ge X L, Yue X F, Wang B Y, et al. Beam spreading and phase singularities' behavior of non-diffracting vortex beams through turbulent atmosphere[J]. *Acta Optica Sinica*, 2019, 39(9): 0901001.
葛筱璐, 岳喜福, 王本义, 等. 湍流大气中无衍射涡旋光束的展宽及相位奇点的演化[J]. *光学学报*, 2019, 39(9): 0901001.
- [2] Cheng Z, Chu X C, Zhao S H, et al. Study of the drift characteristics of Airy vortex beam in atmospheric turbulence [J]. *Chinese Journal of Lasers*, 2015, 42(12): 1213002.
程振, 楚兴春, 赵尚弘, 等. 艾里涡旋光束在大气湍流中的漂移特性研究[J]. *中国激光*, 2015, 42(12): 1213002.
- [3] Jia R, Wei H Y, Zhang H J, et al. Scintillation index of echo wave in slant atmospheric turbulence [J]. *Chinese Journal of Lasers*, 2015, 42(11): 1113001.
贾锐, 韦宏艳, 张洪建, 等. 斜程大气湍流中点目标回波的闪烁研究[J]. *中国激光*, 2015, 42(11): 1113001.
- [4] Ke X Z, Wang C Z. Intensity distribution of the partially coherent vortex beams propagating in atmospheric turbulence[J]. *Laser & Optoelectronics Progress*, 2016, 53(11): 110604.
柯熙政, 王超珍. 部分相干涡旋光束在大气湍流中传输时的光强分布[J]. *激光与光电子学进展*, 2016, 53(11): 110604.
- [5] Ke X Z, Ning C, Wang J. Crosstalk analysis of orbital angular momentum-multiplexed state under atmospheric turbulence [J]. *Infrared and Laser Engineering*, 2018, 47(11): 1122002.
柯熙政, 宁川, 王姣. 大气湍流下轨道角动量复用态串扰分析[J]. *红外与激光工程*, 2018, 47(11): 1122002.
- [6] Yan J L, Wei H Y, Cai D M, et al. Effect of atmospheric turbulence on orbital angular momentum crosstalk of focused vortex beams[J]. *Acta Physica Sinica*, 2020, 69(14): 144203.
闫玠霖, 韦宏艳, 蔡冬梅, 等. 大气湍流信道中聚焦涡旋光束轨道角动量串扰特性[J]. *物理学报*, 2020, 69(14): 144203.
- [7] Lü Q, Sun H L. Study on vortex property of rotating beams in left-handed materials [J]. *Radio Engineering*, 2014, 44(8): 59-62.
吕强, 孙亨利. 左手介质中涡旋电磁波束的涡旋特性研究[J]. *无线电工程*, 2014, 44(8): 59-62.
- [8] Pei S X, Xu S S, Cui F P, et al. Propagation of a Bessel-Gaussian beam in a gradient-index medium [J]. *Applied Optics*, 2019, 58(4): 920-926.
- [9] Li H Y, Liu J W, Bai L, et al. Deformations of circularly polarized Bessel vortex beam reflected and transmitted by a uniaxial anisotropic slab[J]. *Applied Optics*, 2018, 57(25): 7353-7362.
- [10] Liu J W, Li H Y, Li R X, et al. Reflection and transmission of a Bessel vortex beam by a stratified uniaxial anisotropic slab[J]. *Journal of Quantitative Spectroscopy and Radiative Transfer*, 2020, 251: 107046.
- [11] Li H Y, Honary F, Wu Z S, et al. Reflection and transmission of Laguerre-Gaussian beams in a dielectric slab [J]. *Journal of Quantitative Spectroscopy and Radiative Transfer*, 2017, 195: 35-43.
- [12] Li H Y, Honary F, Wang J J, et al. Intensity, phase, and polarization of a vector Bessel vortex beam through multilayered isotropic media [J]. *Applied Optics*, 2018, 57(9): 1967-1976.
- [13] Mario K, Robert F, Matthias F, et al. Communication with spatially modulated light through turbulent air across vienna[J]. *New Journal of Physics*, 2014, 16(11): 113028.
- [14] Sun R D, Guo L X, Cheng M J, et al. Identifying orbital angular momentum modes in turbulence with high accuracy via machine learning [J]. *Journal of Optics*, 2019, 21(7): 075703.
- [15] LeCun Y, Bottou L, Bengio Y, et al. Gradient-based learning applied to document recognition [J]. *Proceedings of the IEEE*, 1998, 86(11): 2278-2324.
- [16] Ebrahim M, Al-Ayyoub M, Alsmirat M A. Will transfer learning enhance ImageNet classification accuracy using ImageNet-pretrained models? [C] // 2019 10th International Conference on Information and Communication Systems (ICICS), June 11-13, 2019, Irbid, Jordan. New York: IEEE Press, 2019: 211-216.
- [17] Lin X, Rivenson Y, Yardimci N T, et al. All-optical machine learning using diffractive deep neural networks[J]. *Science*, 2018, 361(6406): 1004-1008.
- [18] Xie S N, Girshick R, Dollár P, et al. Aggregated residual transformations for deep neural networks[C] // 2017 IEEE Conference on Computer Vision and Pattern Recognition (CVPR), July 21-26, 2017, Honolulu, HI, USA. New York: IEEE Press, 2017: 5987-5995.
- [19] Zhang X P, Huang S, Zhang X H, et al. Residual

- inception: a new module combining modified residual with inception to improve network performance[C]// 2018 25th IEEE International Conference on Image Processing (ICIP), October 7-10, 2018, Athens, Greece. New York: IEEE Press, 2018: 3039-3043.
- [20] Ren S Q, He K M, Girshick R, et al. Faster R-CNN: towards real-time object detection with region proposal networks[J]. IEEE Transactions on Pattern Analysis and Machine Intelligence, 2017, 39(6): 1137-1149.
- [21] Peng Y M, Xue Y, Xiao G Z, et al. Spiral spectrum analysis and application of coherent synthetic vortex beams [J]. Acta Physica Sinica, 2019, 68(21): 214206.
彭一鸣, 薛煜, 肖光宗, 等. 相干合成涡旋光束的螺旋谱分析及应用研究[J]. 物理学报, 2019, 68(21): 214206.
- [22] Jiang Y S, Wang S H, Zhang J H, et al. Spiral spectrum of Laguerre-Gaussian beam propagation in non-Kolmogorov turbulence [J]. Optics Communications, 2013, 303: 38-41.
- [23] Bo B, Menke N, Zhao J L, et al. Generation of vortex beams with a reflected type phase only LCSLM[J]. Journal of Optoelectronics•Laser, 2012, 23(1): 74-78.
薄斌, 门克内木乐, 赵建林, 等. 用反射式纯相位液晶空间光调制器产生涡旋光束[J]. 光电子·激光, 2012, 23(1): 74-78.
- [24] Qi X Q, Gao C Q, Liu Y D. Generation of helical beams with pre-determined energy distribution based on phase modulation gratings [J]. Acta Physica Sinica, 2010, 59(1): 264-270.
齐晓庆, 高春清, 刘义东. 利用相位型衍射光栅生成能量按比例分布的多个螺旋光束的研究[J]. 物理学报, 2010, 59(1): 264-270.
- [25] Li H L, Yang D X, Ren X Y, et al. Experimental investigation of optical vortex generated by volume holography[J]. Acta Optica Sinica, 2010, 30(2): 503-507.
李海莲, 杨德兴, 任小元, 等. 体全息产生光学涡旋的实验研究[J]. 光学学报, 2010, 30(2): 503-507.
- [26] Turnbull G A, Robertson D A, Smith G M, et al. The generation of free-space Laguerre-Gaussian modes at millimetre-wave frequencies by use of a spiral phaseplate[J]. Optics Communications, 1996, 127(4/5/6): 183-188.
- [27] Li W L, Peng T R, Ma J Q. Analysis of influencing factors on quality of Bessel beam generated by deformable mirror[J]. Acta Optica Sinica, 2019, 39(8): 0826003.
李文来, 彭泰然, 马剑强. 变形镜生成贝塞尔光束的质量影响因素分析[J]. 光学学报, 2019, 39(8): 0826003.
- [28] Li P, Zhang S L, Wang S, et al. High efficiency vortex beam generation by optimization of defect-spot mirror[J]. Chinese Journal of Lasers, 2020, 47(5): 0501005.
李平, 张澍霖, 汪莎, 等. 通过优化损耗点镜产生高效率的涡旋光束[J]. 中国激光, 2020, 47(5): 0501005.
- [29] Qin Y L, Huang Y, Tu P, et al. Fabrication of perfect vortex beam microplate using direct laser writing[J]. Chinese Journal of Lasers, 2020, 47(7): 0702003.
秦燕亮, 黄轶, 涂谱, 等. 激光直写制备完美涡旋光束微波带片[J]. 中国激光, 2020, 47(7): 0702003.

Disturbance Orbital Angular Momentum Spectrum Recognition Based on ResNeXt Network

Wu Qiong, Li Haiying^{*}, Ding Wei, Bai Lu, Wu Zhensen

School of Physics and Optoelectronic Engineering, Xidian University, Xi'an, Shaanxi 710071, China

Abstract

Objective Vortex beams carrying orbital angular momentum (OAM) mode have important application prospects in improving communication capacity, multiple-channel information modulation with the same frequency and time. As the vortex beam propagates through complex medium environments, the beam field amplitude and phase may be disturbed, causing channel crosstalk and high bit error rate. Several studies proved that the OAM spectrum disturbance caused by a complex medium environment is one of the key problems that need to be solved in the OAM multiplexing technology. The distribution of the vortex beam's OAM spectrum can easily be obtained through the numerical method. However, the accurate inversion of the OAM spectrum distribution according to the measured

field in the actual measurement system is still worth investigating and discussing. Existing methods for classifying OAM mode mainly focus on the main mode. This study proposes a method for identifying the OAM spectrum distribution of the measured image of the disturbed field using the ResNeXt network. Converting the problem of OAM spectrum distribution to the probability problem discriminates test samples belonging to training samples of each type in convolutional neural network(CNN), and the percentage of the main mode and side lobes of the OAM modal can be obtained.

Methods By optimizing the ResNeXt network, the fitting function of the OAM spectrum distribution of the vortex beam's transmission field calculated from the spectrum analysis theory of vortex beams is set as the self-defined loss function of the network. The total loss function of the network L_{total} consists of three parts. L_1 is the cross-entropy function, which calculates the main mode classification loss of the test sample. $L_2 + L_3$ are the loss functions for predicting the OAM spectrum distribution, and the custom loss function is included in L_2 . L_3 is the cross-entropy function, the same as L_1 . The training samples are the light intensity pattern of a Bessel vortex beam with $l = 4-12$, which does not propagate through the glass medium without aberration. The test samples are the light density diagrams of a Bessel vortex beam with $l = 4$, propagating through an isotropic glass plate with a thickness of 4 mm under different incident angles. The optimized ResNeXt network must first test the category of test samples, called the main mode discrimination. Then, it sets the network study according to the preset fitting function of the OAM spectrum distribution (the self-defined loss function) and obtains the probability that test samples belong to training samples in each category, achieving the purpose of reconstructing the OAM spectrum distribution of the beam's transmission field.

Results and Discussions The discriminating results of the OAM spectrum of the Bessel vortex beam's transmission field are compared with the numerical results based on the ResNeXt network by using a fixed recognition process (Table 1), and light density diagrams of the eighth-order Bessel vortex beam propagate through a glass medium under different incident angles as test samples (Fig. 3). Additionally, the relative errors are calculated (Fig. 4). Since the diffusion of the OAM spectrum distribution increases with an increase in the incident angle, the main mode loses its dominance when the incident angle increases to a certain degree. The proportion of side lobes exceeds the main mode, and the spectrum distribution's regularity is weakened. The ResNeXt network's discriminating error also has an increasing tendency with an increase in the incident angle. However, the maximum relative error does not exceed 22.86% compared with numerical results, and the absolute error of side lobes does not exceed 22.23% (Table 4). There are three main reasons. First, since the Bessel beam has the characteristics of multi-topological charges, its OAM spectrum distribution extends infinitely to both sides with the position of the main mode in the center. However, the training set types are limited and can only be discussed in the main modes. Second, since the regularity of the OAM spectrum distribution of the Bessel vortex beam's transmission field decreases with an increase in the incident angle, the dispersion becomes more obvious, decreasing the recognition accuracy. Finally, since the OAM spectrum recognition problem is different from the conventional classification problem, the CNN feature of test samples is relatively related to the main mode and weakly related to the side lobes. Although the custom loss function contributes to reducing the error, it cannot determine the recognition result of the network. Thus, the side lobe recognition error is greater than the main mode.

Conclusions Based on the ResNeXt network and by introducing self-defined loss function, this study discriminates the OAM spectrum distribution of the Bessel vortex beam's transmission field, which propagates through the glass medium with an incident angle ranging from $0^\circ \sim 45^\circ$, the comparison is made, and the error of the numerical result is analyzed. The results show that the relative error of the main mode increases along with the increase in the wave beam incident angle. However, it does not exceed 22.86%, and the discriminating error of side lobes is bigger than that of the main mode. The proposed method is not limited to the category discrimination of the main mode, but discriminates the percentage of the main mode in the OAM spectrum distribution in detail. This study provides a new idea for the OAM mode discrimination; however, how to improve the discriminating accuracy of side lobes will be the next challenge.

Key words optical communications; vortex Bessel beam; orbital angular momentum; spiral spectrum; neural network; transmitted field

OCIS codes 060.4510; 100.4996; 100.3008